THE JOURNAL OF PHYSICAL CHEMISTRY B

ARTICLE

pubs.acs.org/JPCB

Floquet Analysis for Vibronically Modulated Electron Tunneling

Horacio Carias,[*,†] David N. Beratan,[*,‡] and Spiros S. Skourtis[*,¶]

[†]Department of Physics, Duke University, Durham, North Carolina 27708, United States

[‡]Departments of Chemistry, Biochemistry, and Physics, Duke University, Durham, North Carolina 27708, United States

[¶]Department of Physics, University of Cyprus, Nicosia 1678, Cyprus

Supporting Information

ABSTRACT: Electron tunneling provides the primary reaction channel for electron transfer (ET) in many molecular systems. The analysis of such systems therefore requires the consideration of electronic coherence and interference effects. A model system for which tunneling may be either symmetry forbidden or allowed is considered here in the presence of a driving infrared (IR) field. It was previously shown that inelastic tunneling allows ET in the symmetry forbidden system via vibronic interactions. We show here that explicit considerations of IR interactions with these systems further changes the ET kinetics. Analysis in the framework of Floquet theory reveals that interaction with an IR field may increase the probability of inelastic tunneling and thus enhance the ET rate for a system in which elastic ET is forbidden. It is shown that IR driving of a nuclear oscillator promotes the oscillator into excited states that couple more strongly to the tunneling electron. Furthermore, it is shown that IR driving may suppress the ET rate in this same system, depending on system energetics. In a model where elastic tunneling is symmetry allowed, we examine vibronic modulation of ET in the Floquet framework. ET rates are computed for symmetry allowed and forbidden model systems, and vibronic interactions are found to suppress or enhance ET in both systems. The inelastic ET rate may be enhanced over 4 orders of magnitude in the symmetry disfavored case or suppresed by 15% in the same system. Effects of IR on ET rates in the symmetry-allowed system are weaker with enhancements up to 34% over the undriven rate and suppression of about 3% with IR driving present. This study is the first theoretical and computational exploration of ET rate control by IR irradiation of the bridge.

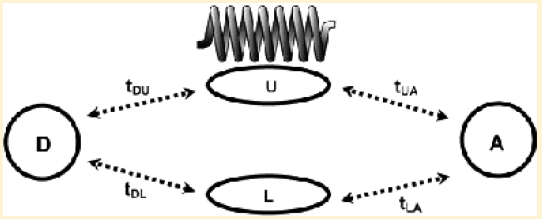

INTRODUCTION

Electron transfer (ET) through molecules can be modulated by inelastic interactions.[1−4] These interactions may be of use to control charge flow through molecules (see refs 1, 2, and 4−9 for example). The aim of this paper is to explore infrared (IR) control of electronic coupling pathway interferences and to understand the way that IR may thus change electron-transfer kinetics.

A particularly intriguing feature of nonadiabatic ET in molecules is electronic[10,11] and vibronic coupling pathway interference.[7,12−14] That is, coupling pathways may interfere constructively or destructively, changing the ET rate accordingly.[3,4,10,11,15−22] Previously, we analyzed a model in which vibronic interactions can erase tunneling pathway interferences in multiply bridged donor-bridge-acceptor systems.[7,12,13]

To explore tunneling in IR-driven systems, we construct a modified version of the model Hamiltonian of ref 12. The system consists of four tight binding electronic sites: a donor site, an acceptor site and two bridge sites. Donor and acceptor both couple to the bridge groups but do not couple directly to each other. The relative sign of these electronic couplings determines whether elastic tunneling is symmetry allowed or forbidden. Additionally, the upper bridge site is linearly coupled to an oscillator. The present treatment differs from that in ref 12 by the inclusion here of a continuous IR driving field that is used to control inelastic tunneling pathway interference.

The dynamics of the system studied here bears a resemblance to systems explored in the field of coherent control, first proposed in the mid-1980s.[23,24] Reactions that form desired products often compete with alternative pathways that lead to other products. By preparing chemical reactants in an excited electronic state whose geometry is close to that of the targeted product, the probability of forming the chosen product is increased. Laser pulses exciting a molecule may introduce new pathways to products, and tuning the phase differences among coherent paths may suppress or enhance product formation based on interference effects. Indeed, experiments have confirmed the theoretical framework for coherent control.[25,26]

Inelastic tunneling provides a means for electron tunneling to proceed in systems where elastic tunneling is symmetry forbidden, that is, for systems where elastic pathways interfere destructively.[12,13] Can we actively promote or control tunneling via these inelastic channels? Consideration of the physical issues and the relevant parameters

Special Issue: Shaul Mukamel Festschrift

Received: November 20, 2010
Revised: March 6, 2011
Published: April 08, 2011

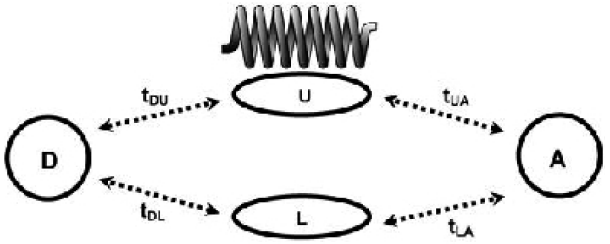

Figure 1. Model System: donor−bridge−acceptor system with upper (U) and lower (L) bridges. The oscillator couples only to the upper bridge electronic state.

leads one to conclude that the answer is yes. The probability of inelastic tunneling is dependent on the strength of vibronic coupling (γ) and is also proportional to the vibrational quantum number m (i.e, $\propto \gamma^2 m$). Thus, exciting vibronically coupled bridge modes will increase the strength of vibronic coupling and thus enhance the probability of bridge-mediated inelastic tunneling.

We propose a method for IR control of electron tunneling that may effectively change the donor−acceptor interactions (and ET kinetics) by modifying vibronic pathway interferences. IR driving at the resonance frequency of an oscillator coupled to an electron tunneling pathway increases the likelihood of vibronic transitions, leading to changes in coupling pathway interferences and effective coupling strength. These changes may enhance or suppress ET due to symmetry and energy conservation effects, as described below. As reported earlier, vibronic interactions can erase destructive coupling pathway interferences in symmetry forbidden systems and thus enhance the rate of ET, by labeling the path taken by the electron.[7,12,13]

The recent discovery of a system with IR-controlled ET dynamics raises the possibility of new molecular switching mechanisms.[8] By turning on an IR field, tunneling to an acceptor may be enhanced or suppressed depending upon the pathway symmetry and vibronic interactions. Additionally, systems with multiple bridges to different acceptors may be controlled by exciting specific localized modes. Exploration of the IR selection of ET pathways and of IR-controlled ET dynamics is in its infancy. IR control of ET is particularly appealing as it affords a lower-energy regime strategy for controlling electronic dynamics compared to electronic excitation.

The effects of dephasing[27,28] will not be considered here, although others have shown that dephasing may turn on ET in systems where ET is otherwise symmetry forbidden.[14] As well, vibrational relaxation is not accounted for here. With typical vibrational state lifetimes in the picosecond domain, ET control by vibrational excitation must be targeted at the ultrafast time scale.

THEORY OF INELASTIC ELECTRON TRANSFER COUPLED TO BRIDGE-LOCALIZED VIBRATIONAL MODES

The rate of nonadiabatic ET coupled to bridge vibrational modes is given by eq 1.[3,12,13,29,30] Here i and f are initial and final vibrational states, respectively. T_{DA} is the electronic coupling between donor and acceptor and ρ_{if} is the Franck-Condon weighted density of states

$$k_{ET} = \sum_i \sum_f P_i k_{DA}^{if} \tag{1}$$

where

$$k_{DA}^{if} = \frac{2\pi}{\hbar}|T_{DA}|^2 \rho_{if} \tag{2}$$

Model Hamiltonian. The full Hamiltonian ($\hat{H}^{syst}$) consists of site electronic energies ($\hat{H}^{e,site}$), hopping interactions among electronic states (ψ) on the donor, bridge and acceptor sites ($\hat{H}^{e,hop}$), a vibrational Hamiltonian for the oscillator on the upper bridge ($\hat{H}^{n}$), and a vibronic interaction between the electron and the bridge oscillator ($\hat{H}^{e/n}$), see Figure 1

$$\hat{H}^{syst} = \hat{H}^{e,site} + \hat{H}^{e,hop} + \hat{H}^{n} + \hat{H}^{e/n} \tag{3}$$

$$\hat{H}^{e,site} = \alpha_D|\psi_D\rangle\langle\psi_D| + \alpha_U|\psi_U\rangle\langle\psi_U| + \alpha_L|\psi_L\rangle \times \langle\psi_L| + \alpha_A|\psi_A\rangle\langle\psi_A| \tag{4}$$

$$\hat{H}^{e,hop} = t_{DU}|\psi_D\rangle\langle\psi_U| + t_{DL}|\psi_D\rangle\langle\psi_L| + t_{UA}|\psi_U\rangle \times \langle\psi_A| + t_{LA}|\psi_L\rangle\langle\psi_A| + hc \tag{5}$$

The vibrational Hamiltonian is either harmonic (as in the top line of eq 6) or anharmonic (as in the bottom line of eq 6). The electron-vibration interaction is taken to be linear (eq 7), allowing only IR-induced transitions between adjacent vibrational states for the harmonic case (nonadjacent couplings were found to have negligible effects for the systems examined here)

$$\hat{H}^{n} = \begin{cases} \sum_m \left(m+\frac{1}{2}\right)\hbar\omega_0|m\rangle\langle m|, & \text{harmonic oscillator} \\ \sum_m \hbar\left[\left(m+\frac{1}{2}\right)\omega_M - \frac{\left(m+\frac{1}{2}\right)^2\omega_M{}^2}{(4D)}\right]|m\rangle\langle m|, & \text{Morse oscillator} \end{cases} \tag{6}$$

Here, ω_0 is the harmonic oscillator frequency. ω_M is the Morse oscillator vibrational constant, and D is the Morse potential well depth.[31] For practical calculations, the number of populated oscillator states is finite (i.e., the infinite vibrational ladder is truncated). In the calculations reported here, the population of oscillator states beyond m = 8 is omitted. Expanding the nuclear Hamiltonian to include higher-energy states does not provide significantly different results (vide infra). The anharmonicity of the Morse potential is necessary to generate ET suppression effects described below. Others have shown that vibrational anharmonicity changes the frequency of electron tunneling oscillations in DBA systems.[32] The linear vibronic interaction Hamiltonian is

$$\hat{H}^{e/n} = \gamma|\psi_U\rangle\langle\psi_U|\sqrt{\frac{2\mu\omega_0}{\hbar}}\,\hat{x} \tag{7}$$

where μ is the reduced mass of the harmonic oscillator. The perturbation of the system by an electromagnetic field is approximated by $\hat{V}^{pert}$ in eq 8

$$\hat{V}^{pert}(t) = -\hat{d}E_0\cos(\omega_d t) \tag{8}$$

E_0 is the amplitude of the driving electric field and ω_d is the frequency of the driving field, set to selectively excite the oscillator from the ground to the first excited state. $\hat{d}$ is the transition dipole operator, parametrized here for an OH oscillator. Only transition elements between adjacent states are included, consistent with a harmonic model.[33]

Floquet Transformation. The resonant and periodic nature of $\hat{V}^{pert}(t)$ lends itself to the use of Floquet analysis (see refs 1, 34−36, and references therein). Floquet theory is particularly

valuable in the regime of resonant excitation because it allows transformation to a differential equation that is periodic in time; this transformation produces a time-independent equation that may be directly diagonalized.[34] The key result of Floquet theory is that the solutions of the time-dependent Schrödinger equation (TDSE) with a time-periodic Hamiltonian $\hat{H}(t) = \hat{H}(t+T)$ are

$$|\Psi_\lambda(t)\rangle = e^{-i\varepsilon_\lambda t/\hbar}|\phi_\lambda(t)\rangle \tag{9}$$

where $|\phi_\lambda(t)\rangle = |\phi_\lambda(t+T)\rangle$ are periodic in time with the same period as the Hamiltonian. Here, $|\phi_\lambda(t)\rangle$ and ε_λ are the eigenvectors and eigenvalues, respectively, of the time-dependent Floquet Hamiltonian $\hat{H}^{\mathrm{F}}(t)$

$$\hat{H}^{\mathrm{F}}(t)|\phi_\lambda(t)\rangle = \varepsilon_\lambda|\phi_\lambda(t)\rangle, \quad \hat{H}^{\mathrm{F}}(t) = \hat{H}(t) - i\hbar\frac{\partial}{\partial t} \tag{10}$$

The solution of the TDSE requires calculation of $|\phi_\lambda(t)\rangle$ and ε_λ via eq 10, and the construction of the time-evolution operator

$$\hat{U}(t) = \sum_\lambda |\Psi_\lambda(t)\rangle\langle\Psi_\lambda(0)| = \sum_\lambda e^{-i\varepsilon_\lambda t/\hbar}|\phi_\lambda(t)\rangle\langle\phi_\lambda(0)| \tag{11}$$

The time periodicity of $\hat{H}$ ($\hat{H}^{\mathrm{F}}$) and of $|\phi_\lambda(t)\rangle$ allows one to write $\hat{H}(t) = \Sigma_k e^{ik\Omega t/\hbar}\,\hat{h}^{(k)}$ and $|\phi_\lambda(t)\rangle = \Sigma_k e^{ik\Omega t/\hbar}\,|c_\lambda^{(k)}\rangle$, where $-\infty < k < \infty$, and $\Omega = 2\pi/T$. Here, $\hat{h}^{(k)}$ and $|c_\lambda^{(k)}\rangle$ are Fourier amplitudes

$$\hat{h}^{(k)} = \frac{1}{T}\int_{-\infty}^{\infty} dt\, e^{-ik\Omega t}\hat{H}(t),$$
$$|c_\lambda^{(k)}\rangle = \frac{1}{T}\int_{-\infty}^{\infty} dt\, e^{-ik\Omega t}|\phi_\lambda(t)\rangle \tag{12}$$

In Floquet analysis, one solves the Fourier transform of eq 10, rather than directly solving eq 10, to find $|\phi_\lambda(t)\rangle$, ε_λ, and the Fourier-amplitude eigenvectors $|c_\lambda^{(l)}\rangle$ and eigenvalues ε_λ. Thus

$$\sum_{l=-\infty}^{\infty} \hat{h}^{\mathrm{F}(k-l)}|c_\lambda^{(l)}\rangle = \varepsilon_\lambda|c_\lambda^{(l)}\rangle, \quad (-\infty \le k(l) \le \infty) \tag{13}$$

where

$$\hat{h}^{\mathrm{F}(k-l)} = \frac{1}{T}\int_{-\infty}^{\infty} dt\, e^{-i(k-l)\Omega t}\hat{H}^{\mathrm{F}}(t)$$
$$= \hat{h}^{(k-l)} + l\hbar\Omega\hat{I}\delta_{k,l} \tag{14}$$

The time-evolution operator (eq 11) is computed by substituting $|\phi_\lambda(t)\rangle = \Sigma_l e^{il\Omega t/\hbar}|c_\lambda^{(l)}\rangle$ in eq 11, while restricting the sum over ε_λ within one Brillouin zone, $(-\hbar\Omega/2 < \varepsilon_\lambda < \hbar\Omega/2)$. If $\hat{H}(t)$ and $|\Psi(t)\rangle = \hat{U}(t)|\Psi(0)\rangle$ are both written in a basis of N system states $\{|\chi_\alpha\rangle\}$, eq 13 is equivalent to the matrix eigenvalue equation, $\mathbf{h}^{\mathrm{F}}\vec{C}_\lambda = \varepsilon_\lambda\vec{C}_\lambda$, where $\mathbf{h}^{\mathrm{F}}$ is an infinite-dimension matrix with elements $\langle\chi_\beta|\hat{h}^{\mathrm{F}(k-l)}|\chi_\alpha\rangle = (1/T)\int_{-\infty}^{\infty} dt\, e^{-i(k-l)\Omega t/\hbar}\,\langle\chi_\beta|\hat{H}^{\mathrm{F}}(t)|\chi_\alpha\rangle$ (described by system and Fourier component indices). $\vec{C}_\lambda$ is an infinite-dimension vector with elements $\langle\chi_\beta|c_\lambda^{(l)}\rangle = (1/T)\int_{-\infty}^{\infty} dt\, e^{-il\Omega t/\hbar}\,\langle\chi_\beta|\phi_\lambda(t)\rangle$. The above methodology may be derived by defining a product Hilbert space of system and driving-field states, that is, $\langle\langle x,t|\Psi,k\rangle\rangle = \langle x|\Psi(t)\rangle \otimes \langle t|k\rangle$, where $\langle t|k\rangle = e^{ik\Omega t}$. Defining the Floquet inner product as the integral

$$\langle\langle\Psi',k'|\Psi,k\rangle\rangle = \frac{1}{T}\int_0^T dt\int_{-\infty}^{\infty} dx\langle k'|t\rangle\langle t|k\rangle\langle\Psi'(t)|x\rangle\langle x|\Psi(t)\rangle \tag{15}$$

we have $\langle\chi_\beta|\hat{h}^{\mathrm{F}(k-l)}|\chi_\alpha\rangle = \langle\langle\chi_\beta,k|\hat{H}^{\mathrm{F}}(t)|\chi_\alpha,l\rangle\rangle$ and $\langle\chi_\beta|c_\lambda^{(l)}\rangle = \langle\langle\chi_\beta, l|\phi_\lambda\rangle\rangle$. Therefore $\mathbf{h}^{\mathrm{F}}\vec{C}_\lambda = \varepsilon_\lambda\vec{C}_\lambda$ is the matrix representation of eq 10 in terms of the Floquet states. In the Floquet representation, the matrix elements of the time-evolution operator (eq 11) among system states $\{|\chi_\alpha\rangle\}$ are

$$\langle\chi_\beta|\hat{U}(t)|\chi_\alpha\rangle = \sum_k e^{ik\Omega t}\sum_{\lambda_{\mathrm{B}},l} e^{-i\varepsilon_{\lambda_{\mathrm{B}},l}t/\hbar}\langle\langle\chi_\beta,k|\phi_{\lambda_{\mathrm{B}}},l\rangle\rangle\langle\langle\phi_{\lambda_{\mathrm{B}}},l|\chi_\alpha\rangle\rangle$$
$$= \sum_k e^{ik\Omega t}\langle\langle\chi_\beta,k|e^{-i\hat{H}^{\mathrm{F}}t/\hbar}|\chi_\alpha,0\rangle\rangle \tag{16}$$

Here, $\varepsilon_{\lambda_{\mathrm{B}},l} = \varepsilon + l\hbar\Omega$ are the infinite eigenvalues of $\mathbf{h}^{\mathrm{F}}$. The λ_{B} sum is restricted to one Brillouin zone $(-\hbar\Omega/2 < \varepsilon_{\lambda_{\mathrm{B}}} < \hbar\Omega/2)$, and the $l(k)$ sums are infinite. For the driven system, $\hat{H}(t) = \hat{H}^{\mathrm{syst}} + \hat{V}^{\mathrm{pert}}(t)$ (eqs 3 and 8), $\Omega = \omega_{\mathrm{d}}$, and the system basis set $\{|\chi_\alpha\rangle\}$ is comprised of the vibronic states $|\psi_{\mathrm{D}}m\rangle = |\psi_{\mathrm{D}}\rangle|m\rangle$, $|\psi_{\mathrm{U(L)}}m\rangle$ and $|\psi_{\mathrm{A}}m\rangle$. Here, ψ denotes donor, bridge, or acceptor electronic states (eq 3); m denotes oscillator states (eq 6). Therefore, the Floquet states are described by three indices (e.g., $|\psi_{\mathrm{D}}m,k\rangle\rangle$), and the matrix $\mathbf{h}^{\mathrm{F}}$ with elements $\langle\langle\chi_\beta,k|\hat{H}^{\mathrm{F}}(t)|\chi_\omega,l\rangle\rangle = \langle\chi_\beta|\hat{h}^{\mathrm{F}(k-l)}|\chi_\alpha\rangle$ is

$$\mathbf{h}^{F} = \begin{bmatrix} \ddots & & \vdots & & & & \iddots \\ & \mathbf{H}^{\mathrm{syst}} - 2\hbar\omega_{\mathrm{d}}\mathbf{I} & \nu & 0 & 0 & 0 & \\ & \nu & \mathbf{H}^{\mathrm{syst}} - \hbar\omega_{\mathrm{d}}\mathbf{I} & \nu & 0 & 0 & \\ \cdots & 0 & \nu & \mathbf{H}^{\mathrm{syst}} & \nu & 0 & \cdots \\ & 0 & 0 & \nu & \mathbf{H}^{\mathrm{syst}} + \hbar\omega_{\mathrm{d}}\mathbf{I} & \nu & \\ & 0 & 0 & 0 & \nu & \mathbf{H}^{\mathrm{syst}} + 2\hbar\omega_{\mathrm{d}}\mathbf{I} & \\ \iddots & & \vdots & & & & \ddots \end{bmatrix} \tag{17}$$

In eq 17

$$\mathbf{H}^{\mathrm{syst}} = \mathbf{H}^{\mathrm{e,site}} + \mathbf{H}^{\mathrm{e,hop}} + \mathbf{H}^{\mathrm{n}} + \mathbf{H}^{\mathrm{e/n}} \tag{18}$$

is the vibronic-state basis matrix representation of the system Hamiltonian (eq 3), and

$$\nu = \frac{1}{T}\int_0^T dt\, e^{-i\omega_{\mathrm{d}}t}\mathbf{V}^{\mathrm{pert}}(t) \tag{19}$$

dx.doi.org/10.1021/jp111097a |J. Phys. Chem. B 2011, 115, 5510–5518

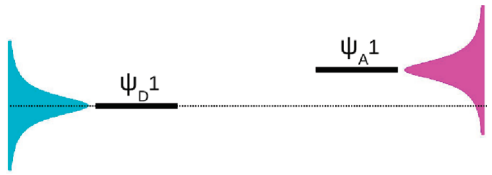

Figure 2. Overlap of broadened donor and acceptor energy levels. The density of states, ρ_{if}, depends on the broadening. The energy difference between initial and final states is denoted δ.

is the Fourier transform of the time-dependent perturbation ($\mathbf{V}^{\mathrm{pert}}$ is the matrix representation of the vibronic basis Hamiltonian in eq 8).

The infinite matrix $\mathbf{h}^{\mathrm{F}}$ in eq 17 is truncated to a 9×9 submatrix where $-4 \le l \le 4$ in the diagonal submatrices $\mathbf{H}^{\mathrm{syst}} + l\hbar\omega_d\mathbf{I}$. Calculations with a larger number of Floquet states do not significantly change the results (i.e., ET rates do not change by more than 1%). Initially, the electron is assumed to be on the donor (ψ_{D}), and the oscillator is in state i. The transition probability from ψ_{D} to ψ_{A} is $P(t)_{\mathrm{D}i\rightarrow\mathrm{A}} = \Sigma_f|\langle\psi_{\mathrm{A}}f|\hat{U}(t)|\psi_{\mathrm{D}}i\rangle|^2$, where f denotes the final state of the oscillator. In terms of the Floquet states

$$P(t)_{\mathrm{D}i\rightarrow\mathrm{A}} = \sum_f \left| \sum_k e^{ik\omega_d t}\langle\langle\psi_{\mathrm{A}}f,k|e^{-i\hat{H}^{\mathrm{F}}t/\hbar}|\psi_{\mathrm{D}}i,0\rangle\rangle \right|^2 \quad (20)$$

where k represents the driving IR field state (eq 16).

The Electron Transfer Rate. To compute an electron transfer rate from eq 20, we add a negative imaginary energy $-i\hbar/t_{\mathrm{r}}$ to the acceptor electronic energy α_{A} in eq 4.[37,38] This term simulates irreversible population relaxation from this state with relaxation rate $1/t_{\mathrm{r}}$[28,39] and energy broadening of the final (acceptor) state relative to the initial (donor) state (Figure 2)

The rate of electron transfer from donor to acceptor is computed from the average time for electrons prepared on the donor to reach the acceptor[37]

$$k_{\mathrm{D}i\rightarrow\mathrm{A}} = \frac{1}{\langle\tau_{\mathrm{D}i\rightarrow\mathrm{A}}\rangle} \quad (21)$$

$$\langle\tau_{\mathrm{D}i\rightarrow\mathrm{A}}\rangle = \frac{\int_0^\infty tP(t)_{\mathrm{D}i\rightarrow\mathrm{A}}\,\mathrm{d}t}{\int_0^\infty P(t)_{\mathrm{D}i\rightarrow\mathrm{A}}\,\mathrm{d}t} \quad (22)$$

The validity of eqs 21 and 22 for describing the ET rate is described in the Supporting Information based on a kinetic model. Equations 21 and 22 give rate constants when relaxation on the acceptor is fast compared with the time scale of electronic amplitude oscillation between donor and acceptor (i.e., $\tau \gg t_{\mathrm{r}}$). τ is determined by the strength of the effective coupling between donor and acceptor (T_{DA}, eq 2). For all calculations reported here, T_{DA} was less than or equal to 4 meV to satisfy the fast relaxation criterion for simple exponential decay, $\tau = \hbar/T_{\mathrm{DA}}$. This magnitude of coupling is typical for organic DBA systems, in which donor and acceptor are separated by 5−6 σ-bonds.[40]

We express the total rate (eq 21) as the sum of individual rates for all possible final states of the oscillator

$$k_{\mathrm{D}i\rightarrow\mathrm{A}} = \sum_f k_{\mathrm{D}i\rightarrow\mathrm{A}f} \quad (23)$$

where the rate contribution from one final oscillator state f is

$$k_{\mathrm{D}i\rightarrow\mathrm{A}f} = \frac{1}{\sigma}\int_0^\infty P(t)_{\mathrm{D}i\rightarrow\mathrm{A}f}\,\mathrm{d}t \quad (24)$$

with $\sigma = \Sigma_f\int_0^\infty tP(t)_{\mathrm{D}i\rightarrow\mathrm{A}f}\,\mathrm{d}t$, and

$$P(t)_{\mathrm{D}i\rightarrow\mathrm{A}f} = \left| \sum_k e^{ik\omega_d t}\langle\langle\psi_{\mathrm{A}}f,k|e^{-i\hat{H}^{\mathrm{F}}t/\hbar}|\psi_{\mathrm{D}}i,0\rangle\rangle \right|^2 \quad (25)$$

In eq 24, the denominator σ contains contributions from all final vibrational states. σ thus normalizes the individual rate contributions (see Supporting Information). The time integrals in eq 24 are computed from the Floquet eigenstates and eigenenergies

$$\int_0^\infty P(t)_{\mathrm{D}i\rightarrow\mathrm{A}f}\,dt = i\sum_{k',\lambda_{\mathrm{B}}',l'}\sum_{k,\lambda_{\mathrm{B}},l}\frac{R^*_{k',\lambda_{\mathrm{B}}',l'}R_{k,\lambda_{\mathrm{B}},l}}{[\varepsilon^*_{\lambda_{\mathrm{B}}',l'} - \varepsilon_{\lambda_{\mathrm{B}},l}]/\hbar - (k'-k)\omega_{\mathrm{d}}} \quad (26)$$

$$\int_0^\infty tP(t)_{\mathrm{D}i\rightarrow\mathrm{A}f}\,dt = -\sum_{k',\lambda_{\mathrm{B}}',l'}\sum_{k,\lambda_{\mathrm{B}},l}\frac{R^*_{k',\lambda_{\mathrm{B}}',l'}R_{k,\lambda_{\mathrm{B}},l}}{\{[\varepsilon^*_{\lambda_{\mathrm{B}}',l'} - \varepsilon_{\lambda_{\mathrm{B}},l}]/\hbar - (k'-k)\omega_{\mathrm{d}}\}^2} \quad (27)$$

where $R_{k,\lambda_{\mathrm{B}},l} = \langle\langle\psi_{\mathrm{A}}f,k|\phi_{\lambda_{\mathrm{B}}},l\rangle\rangle\langle\langle\phi_{\lambda_{\mathrm{B}}},l|\psi_{\mathrm{D}}i,0\rangle\rangle$, and "*" denotes the complex conjugate (the Floquet Hamiltonian is complex because of the imaginary acceptor energy term $-i\hbar/t_{\mathrm{r}}$). All imaginary components in eqs 26 and 27 sum to zero, providing pure real ET rates.

To interpret our calculations, it is helpful to consider a perturbation theory analysis of $k_{\mathrm{D}i\rightarrow\mathrm{A}}$, where the perturbation is the vibronic coupling, $\hat{H}^{\mathrm{e/n}}$. In the weak coupling limit between initial ($|\psi_{\mathrm{D}}i\rangle$) and final ($|\psi_{\mathrm{A}}f\rangle$) vibronic states, $k_{\mathrm{D}i\rightarrow\mathrm{A}f}$ in eq 24 is given approximately by eq 28

$$k^{\mathrm{GR}}_{\mathrm{D}i\rightarrow\mathrm{A}f} = \frac{2\pi}{\hbar}\left|T_{\mathrm{D}i,\mathrm{A}f}\right|^2\rho_{if} \quad (28)$$

where

$$\rho_{if} = \frac{\frac{\hbar}{t_{\mathrm{r}}}}{\pi\left[\left(\frac{\hbar}{t_{\mathrm{r}}}\right)^2 + \delta^2\right]} \quad (29)$$

GR denotes Fermi's golden rule, ρ_{if} is the density of final electronic states (dependent on $\hbar/t_{\mathrm{r}}$), and δ is the energy difference between initial and final vibronic states, (see Supporting Information and Figure 2). $T_{\mathrm{D}i,\mathrm{A}f}$ is the effective bridge-mediated vibronic coupling between $|\psi_{\mathrm{D}}i\rangle$ and $|\psi_{\mathrm{A}}f\rangle$ given by eq 30

$$\begin{aligned} T_{\mathrm{D}i,\mathrm{A}f} &= \langle\psi_{\mathrm{D}}i|\hat{T}^{\mathrm{DA}}|\psi_{\mathrm{A}}f\rangle \\ &= \langle\psi_{\mathrm{D}}|\hat{H}^{\mathrm{e,hop}}|\psi_{\mathrm{U}}\rangle\langle\psi_{\mathrm{U}}i|\hat{G}|\psi_{\mathrm{U}}f\rangle\langle\psi_{\mathrm{U}}|\hat{H}^{\mathrm{e,hop}}|\psi_{\mathrm{A}}\rangle \\ &+ \langle\psi_{\mathrm{D}}|\hat{H}^{\mathrm{e,hop}}|\psi_{\mathrm{L}}\rangle\langle\psi_{\mathrm{L}}i|\hat{G}|\psi_{\mathrm{L}}f\rangle\langle\psi_{\mathrm{L}}|\hat{H}^{\mathrm{e,hop}}|\psi_{\mathrm{A}}\rangle \end{aligned} \quad (30)$$

dx.doi.org/10.1021/jp111097a |J. Phys. Chem. B 2011, 115, 5510–5518

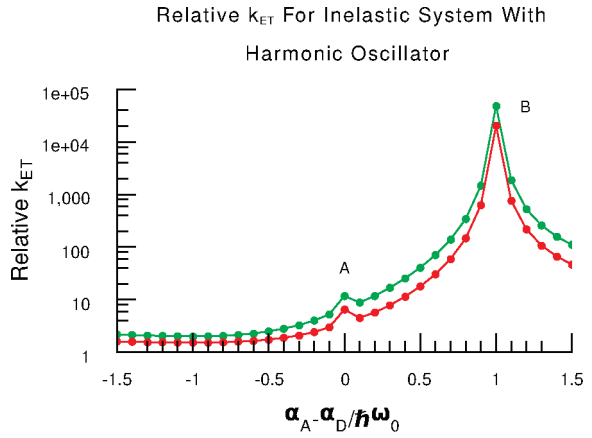

Figure 3. Relative ET rates for an inelastic ET dominated system with a harmonic oscillator. Green represents relative ET rates as defined by eq 36 and red represents rates as defined by eq 35. Peaks A and B for the green (undriven) line are explained in the text, and the contributions from different ET channels $k_{D1\rightarrow A0}$, $k_{D1\rightarrow A1}$, and $k_{D1\rightarrow A2}$ are revealed in Table 1.

where $\hat{G}$ is the bridge vibronic Green's function operator

$$\hat{G}(E) = [E - (\hat{H}^0 + \hat{V})]^{-1} \tag{31}$$

and the zero-order Hamiltonian is the bridge electronic and oscillator Hamiltonian with the vibronic interaction treated as the perturbation

$$\hat{H}^0 = \alpha_U|\psi_U\rangle\langle\psi_U| + \alpha_L|\psi_L\rangle\langle\psi_L| + \hat{H}^n, \quad \hat{V} = \hat{H}^{e/n} \tag{32}$$

In eq 31, E is the tunneling energy of the system (the energy of the initial vibronic state).[41] A perturbative expansion of the bridge vibronic Green's function $\hat{G}$ in terms of $\hat{V}$, that is, eq 33, allows interpretation of $T_{Di,Af}$ as a sum of vibronic coupling pathways.[7,12,13] The perturbative expansion for $\hat{G}$ is

$$\hat{G}(E) = \sum_n \hat{G}^0(E)[\hat{V}\hat{G}^0(E)]^n \tag{33}$$

where

$$\hat{G}^0(E) = (E - \hat{H}^0)^{-1} = \sum_m \left[\frac{|\psi_U m\rangle\langle\psi_U m|}{E - \left[\alpha_U + \hbar\omega_0\left(m + \frac{1}{2}\right)\right]} + \frac{|\psi_L m\rangle\langle\psi_L m|}{E - \left[\alpha_L + \hbar\omega_0\left(m + \frac{1}{2}\right)\right]} \right] \tag{34}$$

and ω_0 is the frequency of the harmonic oscillator (eq 6). To track the influence of intermediate vibronic states that contribute to $k_{Di\Rightarrow A}$, we compute $k_{Di\Rightarrow Af}$ nonperturbatively via eq 24 and the lowest-order contribution to $k^{GR}_{Di\Rightarrow Af}$ in terms of $\hat{H}^{e/n}$. If $k^{GR}_{Di\Rightarrow Af}$ and $k_{Di\Rightarrow Af}$ are similar in magnitude, we interpret the physical basis of the ET rate via vibronic pathway analysis using the Dyson expansion of $\hat{G}$, as shown in eqs 33 and 34.

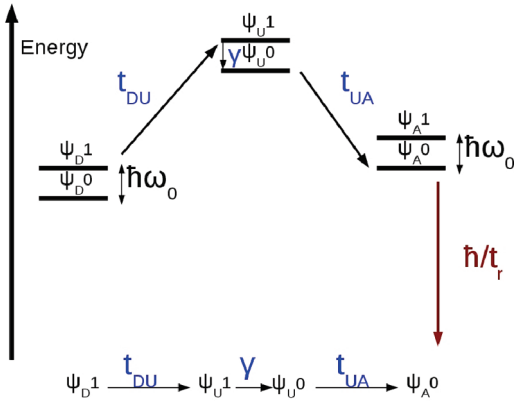

Figure 4. Physical mechanism for enhancement seen in Figure 3, peak B ($k_{D1\rightarrow A0}$ channel). The lowest order vibronic pathway to reach A0 from D1 contributing to $k^{GR}_{D1\rightarrow A0}$ is shown in blue. The total vibronic energy is plotted on the vertical axis. In this case, the $|\psi_D1\rangle$ and $|\psi_A0\rangle$ energies are equal. The schematic mechanism is shown at the bottom of the figure.

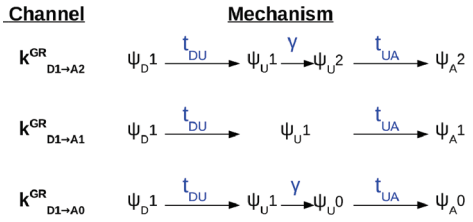

Figure 5. Summary of channels explored in Tables 1−4. The diagrams above represent different terms in the perturbative expansion of T_{DA}. The expansion is in powers of electronic ($\hat{H}^{e,hop}$) and vibronic ($\hat{H}^{e/n}$) off-diagonal Hamiltonian elements (eqs 30−34).

RESULTS AND DISCUSSION

ET rates are first calculated with parameters chosen so that elastic tunneling is forbidden (vide infra). Oscillator parameters are selected to approximate a hydroxyl group (−OH), and the driving field is resonant with the vibrational transition from the ground to the first excited state ($H^n_{1,1} - H^n_{0,0}$ in eq 6).[42] Vibrational relaxation is not introduced to the model. To describe electronic relaxation, a negative imaginary energy is added to the electronic energy of the acceptor ($\alpha_A \Rightarrow \alpha_A - i\hbar/t_r$, vide supra) corresponding to a 1/e decay time of 100 fs. A fast electronic relaxation rate on the acceptor is chosen because the ET dynamics must be fast compared to vibrational relaxation of the bridge oscillator for the rate to be strongly influenced by vibronic excitation. Otherwise, the oscillator would relax before the excited oscillator state could interact with the electron. The short electronic lifetime justifies the absence of an explicit treatment of vibrational relaxation for the bridge. ET rates for a system similar to the one above, in which elastic ET is allowed, were also analyzed (see Figures 7 and 8). In all plots, red lines indicate relative k_{ET} rates defined by eq 35 and green lines indicate relative k_{ET} rates defined by eq 36

$$k^{rel}_{ET} = \frac{k^{d}_{D0\Rightarrow A}}{k^{u}_{D0\Rightarrow A}} \tag{35}$$

$$k^{rel}_{ET} = \frac{k^{u}_{D1\Rightarrow A}}{k^{u}_{D0\Rightarrow A}} \tag{36}$$

dx.doi.org/10.1021/jp111097a |J. Phys. Chem. B 2011, 115, 5510–5518

Table 1. ET Rate Pathway Analysis for Figure 3[a]

rate(/s)	Figure 3 peak A	Figure 3 peak B
$k_{D1\rightarrow A}$	1.43×10^5	6.93×10^7
$k_{D1\rightarrow A0}$	2.46×10^4	6.92×10^7
$k_{D1\rightarrow A1}$	1.07×10^5	
$k_{D1\rightarrow A2}$	1.14×10^4	
$k^{GR}_{D1\rightarrow A0}$	2.47×10^4	6.96×10^7
$k^{GR}_{D1\rightarrow A1}$	1.07×10^5	
$k^{GR}_{D1\rightarrow A2}$	1.15×10^4	

[a] ET rate contributions calculated by Floquet and Green's function methods. $k_{D1\rightarrow A}$ gives the total rate calculated via eqs 21 and eq 23, $k_{D1\rightarrow Ai}$ gives the rate to the final vibronic state $|\psi_A i\rangle$ via eq 24. $k^{GR}_{D1\rightarrow Ai}$ gives the rate to final vibronic state $|\psi_A i\rangle$ via eq 28 and its perturbative analysis, eqs 30−34.

The superscripts d and u in eq 35 and eq 36 indicate IR driven and undriven systems, respectively. The relative rates in eqs 35 and 36 are calculated nonperturbatively using eqs 21 and 26. In all plots with IR driving (red), a laser intensity of 8×10^8 W/m^2 is used, near the limit of what is currently possible with continuous wave lasers. The vibronic channels ($|\psi_D i\rangle \Longrightarrow |\psi_A f\rangle$) that contribute to peaks and dips seen in Figures 3−8 are interpreted using eqs 21 and 30 The coupling mechanisms underlying these pathways are derived by comparing the contributing vibronic channels $k_{Di\Rightarrow Af}$ to the perturbative $k^{GR}_{Di\Rightarrow Af}$ values using eqs 28−34. That is, $k_{Di\Rightarrow Af}$ is recalculated by expanding $T_{Di,Af}$ to lowest nonvanishing order in the vibronic coupling via eqs 33 and 34. This approach is used to explain peaks and dips in the undriven case (green plots); the analogous peaks and dips in the driven case (red plots) cannot be explained by this perturbative strategy because vibrational transitions can also occur via the nonperturbative electromagnetic coupling. Peaks and dips are labeled sequentially from left to right in each plot. Tables accompanying each plot give the rate contribution from three different channels, and Figure 5 summarizes the physical mechanism for each of these channels.

Relative ET Rates for a Symmetry Forbidden System. ET rates were calculated for different $\alpha_A - \alpha_D$ values. The plots in Figure 3 were prepared for symmetry forbidden elastic tunneling ($t_{DU} = t_{DL} = t_{UA} = -t_{LA} = 0.02$ eV, $\gamma = 0.02$ eV), henceforth referred to as the inelastic ET dominated system. Hopping parameters in this range correspond to tunneling through 3−4 bridge σ-bonds.[40]

When the oscillator begins in an excited state for a range of donor−acceptor energy differences between $\pm\hbar\omega_0$, a rate enhancement is seen, as expected. These differences from the undriven ET rate are most pronounced near $\alpha_A = \alpha_D + \hbar\omega_0$ and $\alpha_A = \alpha_D$, due to energy matching between initial and final vibronic states. When the dominant channel in the undriven case produces energy matching between the initial and final vibronic states, the addition of IR driving may break this energy matching and thus result in a decreased rate. Conversely, if the dominant channel in the undriven case is between initial and final vibronic states that are not in resonance, IR driving may create a channel that provides energy matching and thus greatly enhances the rate. Clearly, the rate modification by IR is much larger when the acceptor electronic energy is much greater than the donor energy compared to thermal energies (Figure 3). These uphill processes are unlikely to occur in undriven systems at low temperatures. In this regime, electron−nuclear interaction provides the electron

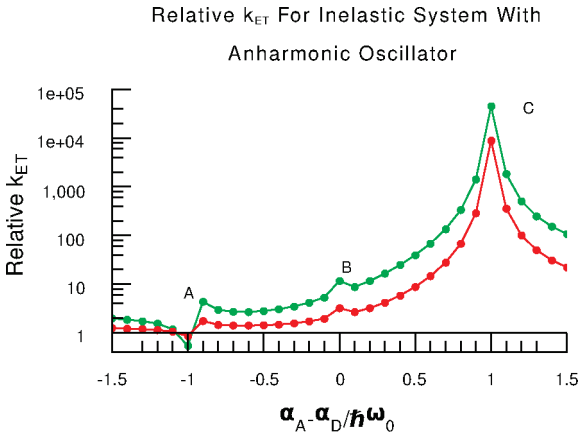

Figure 6. Relative ET rates for the inelastic ET dominated system coupled to an anharmonic oscillator. The green curve represents relative ET rates defined by eq 36 and red represents rates defined by eq 35. Dip A and peaks B and C for the green (undriven) line are explained in the text, and the contributions from different ET channels ($k_{D1\rightarrow A0}$, $k_{D1\rightarrow A1}$, and $k_{D1\rightarrow A2}$) are indicated in Table 2. In this figure, $\hbar\omega_0$ should be interpreted as the energy spacing between the first excited state and the ground state of the anharmonic oscillator Hamiltonian in eq 6.

Table 2. ET Rate Pathway Analysis for Figure 6[a]

rate(/s)	Figure 6 dip A	Figure 6 peak B	Figure 6 peak C
$k_{D1\rightarrow A}$	8.80×10^6	1.46×10^5	6.76×10^7
$k_{D1\rightarrow A0}$		2.52×10^4	6.75×10^7
$k_{D1\rightarrow A1}$		1.07×10^5	
$k_{D1\rightarrow A2}$	8.78×10^6	1.32×10^4	
$k^{GR}_{D1\rightarrow A0}$		2.53×10^4	6.79×10^7
$k^{GR}_{D1\rightarrow A1}$		1.08×10^5	
$k^{GR}_{D1\rightarrow A2}$	8.67×10^6	1.33×10^4	

[a] ET rate contributions calculated by Floquet and Green's function methods. $k_{D1\rightarrow A}$ gives the total rate calculated via eqs 21 and 23, $k_{D1\rightarrow Ai}$ gives the rate to the final vibronic state $|\psi_A i\rangle$ *via* eq 24. $k^{GR}_{D1\rightarrow Ai}$ gives the rate to final vibronic state $|\psi_A i\rangle$ via eq 28 and its perturbative analysis.

with energy for an otherwise uphill process. The stronger effect seen when EM driving is present (red) is due to vibronic interactions with an oscillator excited beyond the first excited state. Recall the $\gamma^2 m$ scaling of the inelastic tunneling transition probabilities. The relative enhancement of the driven vs undriven plots reaches its maximum ratio of 2.7 when donor and acceptor electronic energies are equal, $\alpha_A = \alpha_D$.

As shown in Table 1, considering only the oscillator ground state ($f = 0$) in eq 23, peak B at $\alpha_A = \alpha_D + \hbar\omega_0$ for the undriven (green) case is shown to arise primarily from vibronic interactions. In the vibronic channel $k_{D1\rightarrow A0}$ (Table 1), the electron gains energy from the oscillator, thereby bringing the oscillator down to the ground state and giving the electron the energy to match the acceptor electronic state energy, that is, $|\psi_D 1\rangle \Longrightarrow |\psi_A 0\rangle$. The $k_{D1\rightarrow A0}$ channel makes the only non-negligible contribution to peak B (see Table 1). The paths where the vibronic interactions relax the oscillator and impart $\hbar\omega_0$ to the electron ($k^{GR}_{D1\rightarrow A0}$ in Table 1) dominate the $k_{D1\rightarrow A0}$ channel.

Peak A at $\alpha_A = \alpha_D$ in Figure 3 is somewhat less intuitive in its origins than peak B. Perturbative (GR) analysis shows that the

dx.doi.org/10.1021/jp111097a |*J. Phys. Chem. B* 2011, 115, 5510–5518

dominant vibronic channel arises from two vibronic interactions ($\hat{H}^{e/n}$) with no net change in the electronic energy (a similar mechanism was described for STM[43]) However, two other pathways also provide a significant contribution to the rate. One pathway involves the flow of energy from the electron to the oscillator, and the other involves the flow of energy to the electron from the oscillator. Together, these two paths account for 25% of the total ET rate.

The case of an anharmonic oscillator shown in Figure 6 is very similar to the harmonic case, and the peaks in the figure, analogous to those in Figure 3, arise from similar physical mechanisms. In Figure 6, $\hbar\omega_0$ should be interpreted as the energy spacing between the first excited state and the ground state of the anharmonic oscillator in eq 6 (the difference $H^n_{1,1} - H^n_{0,0}$ for the anharmonic Hamiltonian). Dip A near $\alpha_A = \alpha_D - \hbar\omega_0$ is explained by the anharmonicity of the oscillator; when the oscillator begins in the ground state, the electron may excite it to the first excited state, thus losing just enough energy to match the acceptor electronic state energy. However, if the oscillator is in an excited state when the electron excites it, the electron no longer loses exactly enough energy to be in resonance with the acceptor electronic energy because the vibrational level spacings for the anharmonic oscillator depend on the degree of excitation, that is, $H^n_{2,2} - H^n_{1,1} \neq H^n_{1,1} - H^n_{0,0}$. Thus, we find that IR driving of an ET system coupled to an anharmonic oscillator may retard the ET rate for these donor−acceptor energy differences.

Relative ET Rates for Symmetry Allowed System. A model system was built, similar to the symmetry forbidden case considered in Section 3.1, where elastic tunneling is symmetry allowed ($t_{DU} = t_{DL} = t_{UA} = t_{LA} = 0.02$ eV and $\gamma = 0.02$ eV). This system is referred to as the "elastic ET dominated system". As in the inelastic ET dominated system, rates are calculated for the system without IR driving and with the oscillator in an excited state, as well as for the oscillator beginning in the ground state with IR driving.

For the elastic ET dominated system, we find that IR driving of a harmonic oscillator has little effect on the kinetics except to establish peaks or dips near $\alpha_A = \alpha_D \pm \hbar\omega_0$ that arise from energy matching constraints on the initial and final vibronic states. For other values of the donor−acceptor energy difference, the ET rate is nearly unchanged, indicating no difference from the system that lacks both IR driving and an excited oscillator. Because elastic ET is allowed in this system, the relative enhancement due to IR driving is not as great as in the inelastic dominated system. The maximum ratio of IR driven ET over undriven ET is 1.2, and it is found at $\alpha_A = \alpha_D + \hbar\omega_0$ (peak B in Figure 7).

Peak A at $\alpha_A = \alpha_D - \hbar\omega_0$ in Figure 7 arises from two channels. The greatest contribution comes from the elastic channel. An inelastic channel also contributes in which vibronic excitation of $\hbar\omega_0$ is imparted to the oscillator, thus lowering the electronic energy by $\hbar\omega_0$ and bringing it into resonance with the acceptor electronic energy (Table 3). Table 3 partitions peak B of Figure 7 at $\alpha_A = \alpha_D + \hbar\omega_0$ into two primary contributions. The elastic channel again provides the largest contribution to the rate, but the path where the electron gains $\hbar\omega_0$ from the oscillator also makes a significant contribution.

Introducing an anharmonic oscillator (Morse oscillator of eq 6 and Figure 8) we find a dip in the relative ET rate at $\alpha_A = \alpha_D - \hbar\omega_0$ (dip A in Figure 8). In Figure 8, $\hbar\omega_0$ should be interpreted as the energy spacing between the first excited state and the ground state of the anharmonic oscillator in eq 6 (the

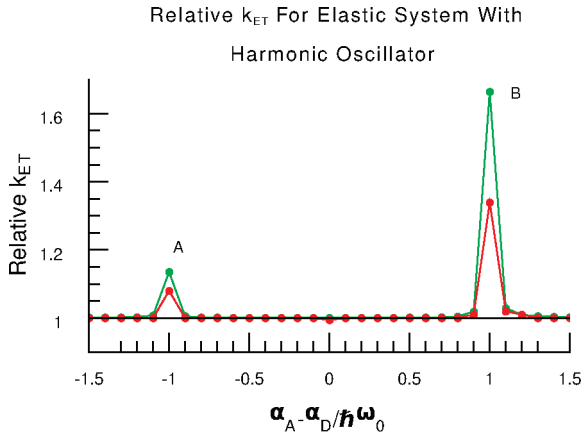

Figure 7. Relative ET rates for elastic ET dominated system with harmonic oscillator. Green represents relative ET rates as defined by eq 36 and red represents rates as defined by eq 35. Peaks A and B for the green (undriven) line are explained in the text, and the contributions from different ET channels $k_{D1\rightarrow A0}$, $k_{D1\rightarrow A1}$, and $k_{D1\rightarrow A2}$ are revealed in Table 3.

Table 3. ET Rate Pathway Analysis for Figure 7[a]

rate(/s)	Figure 7 peak A	Figure 7 peak B
$k_{D1\rightarrow A}$	1.37×10^8	1.73×10^8
$k_{D1\rightarrow A0}$		6.91×10^7
$k_{D1\rightarrow A1}$	1.04×10^8	1.04×10^8
$k_{D1\rightarrow A2}$	3.22×10^7	
$k^{GR}_{D1\rightarrow A0}$		6.96×10^7
$k^{GR}_{D1\rightarrow A1}$	1.05×10^8	1.05×10^8
$k^{GR}_{D1\rightarrow A2}$	3.23×10^7	

[a] ET rate contributions calculated by Floquet and Green's function methods. $k_{D1\rightarrow A}$ gives the total rate calculated via eqs 21 and 23, $k_{D1\rightarrow Ai}$ gives the rate to the final vibronic state $|\psi_A i\rangle$ via eq 24. $k^{GR}_{D1\rightarrow Ai}$ gives the rate to the final vibronic state $|\psi_A i\rangle$ via eq 28 and its perturbative analysis.

difference $H^n_{1,1} - H^n_{0,0}$ for the anharmonic Hamiltonian). Dip A arises from the same energy conservation constraints that caused a dip at this energy in the inelastic system with an anharmonic oscillator, Figure 6. The origins of peak B at $\alpha_A = \alpha_D + \hbar\omega_0$ in Figure 8 for the anharmonic oscillator system has the same source as peak B in Figure 7. Dip A at $\alpha_A = \alpha_D - \hbar\omega_0$ has the same source as that in Figure 6, with an additional contribution from an elastic channel. Preparing the anharmonic oscillator in the first excited state precludes the electron from losing the energy difference between the ground and first excited state and thus perfectly matching the acceptor electronic energy.

IR driving (when the oscillator is harmonic) has a greater effect on the rate compared to the case where the oscillator begins in the first excited state and there is no IR driving. The higher vibrational states accessed in the harmonic oscillator have stronger couplings to adjacent states (since the squared transition dipole elements are proportional to the quantum number), and the influence of vibronic coupling grows as the oscillator climbs the vibrational ladder. In the anharmonic oscillator system, all states beyond the first vibrational excited state are off-resonant with the driving IR field and thus are not accessed by monochromatic IR driving. Within the golden rule parameter regime

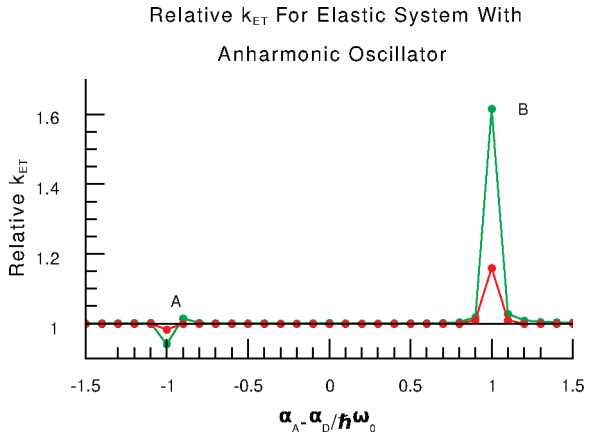

Figure 8. Relative ET rates for elastic ET dominated system with anharmonic oscillator. Green represents relative ET rates as defined by eq 36 and red represents rates as defined by eq 35. Dip A and peak B for the green (undriven) line are explained in the text, and the contributions from different ET channels $k_{D1\rightarrow A0}$, $k_{D1\rightarrow A1}$, and $k_{D1\rightarrow A2}$ are revealed in Table 4. $\hbar\omega_0$ should be interpreted as the energy spacing between the first excited state and the ground state of the anharmonic oscillator in eq 6.

Table 4. ET Rate Pathway Analysis for Figure 8 [a]

rate(/s)	Figure 8 dip A	Figure 8 peak B
$k_{D1\rightarrow A}$	1.18×10^8	1.77×10^8
$k_{D1\rightarrow A0}$		6.74×10^7
$k_{D1\rightarrow A1}$	1.10×10^8	1.10×10^8
$k_{D1\rightarrow A2}$	8.77×10^6	
$k^{GR}_{D1\rightarrow A0}$		6.79×10^7
$k^{GR}_{D1\rightarrow A1}$	1.10×10^8	1.10×10^8
$k^{GR}_{D1\rightarrow A2}$	8.67×10^6	

[a] ET rate contributions calculated by Floquet and Green's function methods. $k_{D1\rightarrow A}$ gives the total rate calculated via eqs 21 and 23, $k_{D1\rightarrow Ai}$ gives the rate to the final vibronic state $|\psi_{Ai}\rangle$ via eq 24. $k^{GR}_{D1\rightarrow Ai}$ gives the rate to final vibronic state $|\psi_{Ai}\rangle$ via eq 28 and its perturbative analysis.

used here, the same qualitative effects are seen with larger and smaller electron-hopping elements. For example, $\hat{H}^{e,hop}$ scaled down by a factor of 10 provides relative driven ET rates ($k^{d}_{D0\Rightarrow A}/k^{u}_{D0\Rightarrow A}$) enhancements/suppressions that are 50−200% greater than those described above, but the undriven relative rates ($k^{u}_{D1\Rightarrow A}/k^{u}_{D0\Rightarrow A}$) are virtually unchanged.

Experimental realizations of the qualitative effects described here could be complicated by many factors. For IR driving of the symmetry forbidden ET system and IR driving of the symmetry allowed system, experiments are likely to be implemented with pulsed rather than continuous excitation.[27] Complications in pulsed experiments include excitation of higher vibrational states due to the multichromatic nature of the pulses. For anharmonic oscillators studied here, states above the first are unpopulated, but real systems would experience excitation to these higher levels because of the laser bandwidth. Vibrational relaxation may also hinder the experimental realization of these effects by relaxing the excited oscillator before it interacts with the electron. Interactions with the solvent will broaden the sharp resonance features described here. Also, vibronic coupling must occur with excited states of the oscillator in order to influence the dynamics with respect to the undriven case. To satisfy this requirement, relaxation of the oscillator must not occur on time scales shorter than the inverse of the ET rate, and typical vibrational lifetimes are on the tens of picoseconds time scale.[28] Finally, for some DBA systems, ET may proceed incoherently; indeed hopping mechanisms were not considered in this study.

CONCLUSIONS

Continuous-wave infrared driving of a vibrational mode coupled to a bridge electronic state in a model system was shown to change the ET rate in DBA systems and to provide a possible means to control ET dynamics. Both ET rate slowing and acceleration are found to be accessible. Analysis of ET pathways via Floquet and Green's function methods indicates that this enhancement arises from the increased vibronic interactions between excited vibrational states and bridge electronic states. Vibronically modulated ET has direct relevance to recent experiments. Experimentally, ET rate lowering was observed with IR driving.[8] Although rate lowering effects were suggested to arise from weakening of electronic coupling caused by vibrational motion, the present study indicates that ET rate lowering may also arise from other sources. We believe that this is the first theoretical demonstration that ET rates may be affected by manipulating vibronic interactions through driving IR fields and that IR excitation may provide a means to control ET.

The calculations reported here reveal that anharmonicity may have a significant impact on IR-modulated ET and may even determine whether IR driving enhances or suppresses ET in otherwise identical electronic systems. Linear versus nonlinear vibronic coupling does not qualitatively alter the effects. The strongest effects found in this study arise when donor and acceptor electronic energies differ by an amount that matches the energy gap between the first vibrational excited state of the oscillator and its ground state. These resonance effects may be challenging to observe in condensed phase experiments because the effects depend on very specific energy differences between donor and acceptor. However, experiments on molecular wires between metal leads indicate that turning on mode-specific transport channels is accessible.[44] Indeed, the results of the present study may be of interest to researchers in inelastic electron tunneling spectroscopy. The ET rate enhancements seen when $\alpha_A = \alpha_D + \hbar\omega_0$ may allow current to flow against an applied bias when IR driving is present in an IET experiment, as IR may overcome the electrochemical bias. However, it is important to note that dissipative effects not considered here may prevent experimental verification of such IET properties.

ASSOCIATED CONTENT

Supporting Information. Vibronic pathway and kinetic model interpretation of results. This material is available free of charge via the Internet at http://pubs.acs.org.

AUTHOR INFORMATION

Corresponding Author

*E-mail: (H.C.) horacio.carias@duke.edu; (D.N.B.) david.beratan@duke.edu; (S.S.S.) skourtis@ucy.ac.cy.

ACKNOWLEDGMENT

The authors acknowledge support of the National Science Foundation (CHE-1012357), including a travel supplement to

H.C. S.S.S. thanks the University of Cyprus for support of this research project. We thank the Duke Nanoscience Program for additional support. We are also indebted to Dequan Xiao, Igor V. Rubtsov, and Abraham Nitzan for many useful discussions.

REFERENCES

(1) Kohler, S.; Lehmann, J.; Hänggi, P. *Phys. Rep.* **2005**, *406*, 379–443.
(2) Galperin, M.; Ratner, M. A.; Nitzan, A. *J. Phys.: Condens. Matter* **2007**, *19*, 111–121.
(3) Skourtis, S. S.; Waldeck, D.; Beratan, D. N. *Annu. Rev. Phys. Chem.* **2010**, *61*, 461–485.
(4) Beratan, D. N.; Skourtis, S. S.; Balabin, I. A.; Balaeff, A.; Keinan, S.; Venkatramani, R.; Xiao, D. *Acc. Chem. Res.* **2009**, *42*, 1669–1678.
(5) Maddox, J. B.; Harbola, U.; Liu, N.; Silien, C.; Ho, W.; Bazan, G. C.; Mukamel, S. *J. Phys. Chem. A* **2006**, *110*, 6329–6338.
(6) Gagliardi, A.; Solomon, G. C.; Pecchia, A.; Frauenheim, T.; Di Carlo, A.; Hush, N. S.; Reimers, J. R. *Phys. Rev. B* **2007**, *75*, 174306.
(7) Xiao, D.; Skourtis, S. S.; Rubtsov, I.; Beratan, D. N. *Nano Lett.* **2009**, *9*, 1818–1823.
(8) Lin, Z.; Lawrence, C. M.; Xiao, D.; Kireev, V. V.; Skourtis, S. S.; Sessler, J. L.; Beratan, D. N.; Rubtsov, I. V. *J. Am. Chem. Soc.* **2009**, *131*, 18060–18062.
(9) Galperin, M.; Ratner, M. A.; Nitzan, A.; Troisi, A. *Science* **2008**, *319*, 1056–1060.
(10) Beratan, D. N.; Hopfield, J. J. *J. Am. Chem. Soc.* **1984**, *106* 1584–1594.
(11) Newton, M. D. *Chem. Rev.* **1991**, *91*, 767–792.
(12) Skourtis, S. S.; Waldeck, D. H.; Beratan, D. N. *J. Phys. Chem. B* **2004**, *108*, 15511–15518.
(13) Skourtis, S. S.; Beratan, D. N. *AIP Conf. Proc.* **2007**, *2*, 809–812.
(14) Goldsmith, R. H.; Wasielewski, M. R.; Ratner, M. A. *J. Phys. Chem. B* **2006**, *39*, 3435–3437.
(15) Sautet, P.; Joachim, C. *Chem. Phys. Lett.* **1988**, *153*, 511–516.
(16) Zeng, Y.; Zimmt, M. B. *J. Am. Chem. Soc.* **1991**, *113*, 5107–5109.
(17) Onuchic, J. N.; Beratan, D. N.; Winkler, J. R.; Gray, H. B. *Rev. Biophys. Biomol. Struct.* **1992**, *21*, 349–377.
(18) Jordan, K. D.; Paddon-Row, M. N. *Chem. Rev.* **1992**, *92*, 395–410.
(19) Reimers, J. R.; Hush, N. S. *Chem. Phys.* **1996**, *208*, 177–193.
(20) Patoux, C.; Coudret, C.; Launay, J.-P.; Joachim, C.; Gourdon, A. *Inorg. Chem.* **1997**, *36*, 5037–5049.
(21) Ke, S.-H.; Yang, W.; Baranger, H. U. *Nano Lett.* **2008**, *8*, 3257–3261.
(22) Solomon, G. C.; Andrews, D. Q.; Hansen, T.; Goldsmith, R. H.; Wasielewski, M. R.; Van Duyne, R. P.; Ratner, M. A. *J. Chem. Phys.* **2008**, *129*, 054701.
(23) Tannor, D. J.; Rice, S. *J. Chem. Phys.* **1985**, *83*, 5013–5018.
(24) Brumer, P.; Shapiro, M. *Chem. Phys. Lett.* **1986**, *126*, 541–546.
(25) Shapiro, M.; Brumer, P. *Principles of the Quantum Control of Molecular Processes*; Wiley: New York, 2003.
(26) Rice, S. A.; Zhao, M. *Optical Control of Molecular Dynamics*; Wiley: New York, 2000.
(27) Mukamel, S. *Principles of Nonlinear Optical Spectroscopy*; Oxford: New York, 1999.
(28) Nitzan, A. *Chemical Dynamics in Condensed Phases*; Oxford Graduate Texts: New York, 2006.
(29) Medvedev, E. S.; Stuchebrukhov, A. A. *J. Chem. Phys.* **1997**, *107*, 3821–3831.
(30) Troisi, A.; Nitzan, A.; Ratner, M. A. *J. Chem. Phys.* **2003**, *119* 5782–5788.
(31) Tran, L. B.; Huffaker, J. N. *J. Math. Phys.* **1983**, *24*, 397–398.
(32) Brisker, D.; Peskin, U. *J. Chem. Phys.* **2006**, *125*, 111103.
(33) Jakubetz, W.; Manz, J.; Mohan, V. *J. Chem. Phys.* **1989**, *7*, 3686–3699.
(34) Shirley, J. H. *Phys. Rev.* **1965**, *138*, B979–B987.
(35) Tikhonov, A.; Coalson, R. D.; Dahnovsky, Y. *J. Chem. Phys.* **2002**, *116*, 10909–10920.
(36) Tannor, D. *Introduction to Quantum Mechanics: A Time-Dependent Perspective*; University Science Books: New York, 2006.
(37) Skourtis, S. S.; Da Silva, A. J. R.; Bialek, W.; Onuchic, J. N. *J. Phys. Chem.* **1992**, *96*, 8034–8041.
(38) Skourtis, S. S.; Nitzan, A. *J. Chem. Phys.* **2003**, *119*, 6271–6276.
(39) Reimers, J. R.; Hush, N. S. *Chem. Phys.* **1989**, *134*, 323–354.
(40) Closs, G. L.; Miller, J. R. *Science* **1988**, *240*, 440–447.
(41) Skourtis, S.; Beratan, D. Electron Transfer-From Isolated Molecules to Biomolecules, Part 1. *Advances in Chemical Physics*; John Wiley & Sons Inc: New York, 1999; Vol. 106, pp 377−452.
(42) Herzberg, G. *Molecular Spectra and Molecular Structure*; Van Nostrand: New York, 1945.
(43) Persson, B. N. J.; Baratoff, A. *Phys. Rev. Lett.* **1987**, *59*, 339–342.
(44) Kiguchi, M.; Tal, O.; Wohlthat, S.; Pauly, F.; Krieger, M.; Djukic, D.; Cuevas, J. C.; van Ruitenbeek, J. M. *Phys. Rev. Lett.* **2008**, *101*, 046801.